Tree Physiology 37, 617–631
doi:10.1093/treephys/tpx002

Research paper

A multi-proxy assessment of dieback causes in a Mediterranean oak species

Michele Colangelo[1], J. Julio Camarero[2], Giovanna Battipaglia[3,4], Marco Borghetti[1], Veronica De Micco[5], Tiziana Gentilesca[1] and Francesco Ripullone[1,6]

[1]School of Agricultural, Forest, Food and Environmental Sciences, University of Basilicata, viale dell'Ateneo Lucano 10, 85100 Potenza, Italy; [2]Pyrenean Institute of Ecology (IPE-CSIC), Avda Montañana 1005, 50192 Zaragoza, Spain; [3]Department of Environmental, Biological and Pharmaceutical Sciences and Technologies, Second University of Naples, Caserta, Italy; [4]École Pratique des Hautes Études (PALECO EPHE), Institut des Sciences de l'Évolution, University of Montpellier 2, F-34090 Montpellier, France; [5]Department of Agricultural Sciences, University of Naples Federico II, Portici (Naples), Italy; [6]Corresponding author (francesco.ripullone@unibas.it)

Received September 6, 2016; accepted January 20, 2017; published online February 9, 2017; handling Editor Roberto Tognetti

Drought stress causes forest dieback that is often explained by two interrelated mechanisms, namely hydraulic failure and carbon starvation. However, it is still unclear which functional and structural alterations, related to these mechanisms, predispose to dieback. Here we apply a multi-proxy approach for the characterization of tree structure (radial growth, wood anatomy) and functioning ($\delta^{13}C$, $\delta^{18}O$ and non-structural carbohydrates (NSCs)) in tree rings before and after drought-induced dieback. We aim to discriminate which is the main mechanism and to assess which variables can act as early-warning proxies of drought-triggered damage. The study was tailored in southern Italy in two forests (i.e., San Paolo (SP) and Oriolo (OR)) where declining and non-declining trees of a ring-porous tree species (*Quercus frainetto* Ten.) showing anisohydric behavior coexist. Both stands showed growth decline in response to warm and dry spring conditions, although the onset of dieback was shifted between them (2002 in SP and 2009 in OR). Declining trees displayed a sharp growth drop after this onset with reductions of 49% and 44% at SP and OR sites, respectively. Further, contrary to what we expected, declining trees showed a lower intrinsic water-use efficiency compared with non-declining trees after the dieback onset (with reductions of 9.7% and 5.6% at sites SP and OR, respectively), due to enhanced water loss through transpiration, as indicated by the lower $\delta^{18}O$ values. This was more noticeable at the most drought-affected SP stand. Sapwood NSCs did not differ between declining and non-declining trees, indicating no carbon starvation in affected trees. Thus, the characterized structural and functional alterations partially support the hydraulic failure mechanism of dieback. Finally, we show that growth data are reliable early-warning proxies of drought-triggered dieback.

Keywords: carbon and oxygen isotopes, climate warming, dendrochronology, non-structural carbohydrates, quantitative wood anatomy, *Quercus frainetto*, southern Italy.

Introduction

Drought and heat stress cause forest dieback worldwide (Allen et al. 2010). However, a multi-proxy picture considering several structural and functional variables (growth, wood anatomy and water-use efficiency (WUE)) to infer how dieback occurs is still lacking. In the Allen et al. (2010) review, only 11% of the dieback cases involved ring-porous oak species with anisohydric behavior, i.e., showing large declines in leaf midday water potential during drought, which are supposed to better able to survive droughts under the forecasted warmer conditions than taller conifer isohydric species (McDowell and Allen 2015). When there is no water restriction, anisohydric species maintain higher stomatal conductance (g) and photosynthesis (A) rates than isohydric tree species, tracking changes in vapor pressure deficit (VPD) and showing little dependence on changes in soil moisture (Klein 2014). However, under intense or prolonged

drought, anisohydric species are prone to xylem cavitation, while isohydric species rapidly close stomata (Klein 2014, Attia et al. 2015). If warmer conditions enhance atmospheric evaporative demand moving VPD toward a critical threshold, then drought stress could be magnified and trigger dieback, making anisohydric species vulnerable (Williams et al. 2013). In the case of ring-porous Mediterranean oak species, extreme droughts may surpass the limit of hydraulic safety at which they often function (Tognetti et al. 1998).

Drought-induced dieback is explained by two non-mutually exclusive mechanisms: (i) hydraulic failure due to a drastic loss of xylem conductivity and (ii) carbon starvation when carbon demands are not met (McDowell et al. 2008, 2011; McDowell 2011). The multiple links between these mechanisms are mediated by structural and functional changes affecting growth, wood anatomy and WUE. Regarding structural changes, wood anatomy is related to the occurrence of hydraulic failure and shoot dieback since wide xylem vessels are more prone to cavitation and loss of hydraulic conductivity than narrow vessels (Nardini et al. 2013). Cavitation resistance is linked to a reduction in lumen area or the mechanical reinforcement of fibers that prevent xylem embolism and drought damage (Hacke et al. 2001). In oaks, a reduction in lumen size of earlywood (EW) vessels and a sharp decrease in latewood (LW) production have been described as wood-anatomical responses to tolerate drought (Corcuera et al. 2004*b*, Eilmann et al. 2009). However, anisohydric oak species also show extensive xylem embolism if water shortage is prolonged (Hoffmann et al. 2011).

Altered structural conditions also include a decline in radial growth and abrupt shifts in climate–growth associations (Pellizzari et al. 2016). For instance, in several oak species, a growth decline and the weakening of climate–growth relationships started in response to severe droughts 20–50 years prior to dieback onset (Dwyer et al. 1995, Drobyshev et al. 2007, Wyckoff and Bowers 2010, Haavik et al. 2011, Gea-Izquierdo et al. 2014, Stojanović et al. 2015). Therefore, the relationships between dieback, growth and wood anatomy may also depend on functional traits affecting water use, and carbon uptake and storage (McDowell et al. 2008).

Water scarcity constrains growth and is responsible for loss in xylem conductivity affecting A and g, thus reducing carbon uptake (Hsiao 1973, Bréda et al. 2006). Mild droughts impair the transport of assimilates through the phloem and trigger the conversion of stored carbon (e.g., starch) into osmolytes (e.g., soluble sugars (SS)) to maintain turgor pressure (Sala et al. 2010, 2012, Pantin et al. 2013). Contrastingly, severe droughts can impair photosynthesis and lead to carbon starvation and dieback (Sevanto et al. 2014). Shifts in intrinsic water-use efficiency (WUE_i), i.e., the A/g ratio, may be inferred through the combined analysis of carbon ($\delta^{13}C$) and oxygen ($\delta^{18}O$) isotope compositions in leaves or tree-ring cellulose, the so-called dual-isotope approach (Scheidegger et al. 2000, Barbour et al. 2002, Ferrio and Voltas 2005, Ripullone et al. 2009, but see Roden and Farquhar 2012). Changes in gas exchange are recorded in tree rings through carbon isotope composition ($\delta^{13}C$), which gives insight into how trees respond to drought (Farquhar et al. 1989, Saurer et al. 2004, Battipaglia et al. 2010). On the other hand, $\delta^{18}O$ is correlated with soil water sources and g, making it a proxy for leaf transpiration and evaporative demand (Saurer et al. 1997).

Here we argue for a multi-proxy characterization of tree structure (i.e., the analysis of stem radial growth and wood-anatomical functional traits) and functioning (i.e., the determination of $\delta^{13}C$, $\delta^{18}O$, WUE_i, non-structural carbohydrates (NSCs)) to determine how water and carbon limitations drive drought-induced dieback (Voltas et al. 2013, Billings et al. 2016). We explore the likely occurrence of structural and functional alterations in a ring-porous tree species (*Quercus frainetto* Ten.) (Chatziphilippidis and Spyroglou 2004) that presents ongoing dieback in southern Italy. This species shows mid to high growth rates and it is very sensitive to dry conditions in late spring and summer, and recovery rates after drought are rapid (Sanders et al. 2014). Since the 1980s, drought-induced dieback episodes have been detected in southern Italian oak forests showing a worrisome trend of increasing damage, as in other areas of the Mediterranean Basin (Ragazzi et al. 1989, Salvatore et al. 2002). We compare declining and non-declining Italian oak trees coexisting at two sites to improve our understanding of dieback.

We hypothesize that declining trees should show higher growth rates, wider lumen areas and stronger climate–growth associations prior to the dieback onset since these features make them more susceptible to drought-induced damage (Levanič et al. 2011). After the dieback onset, we expect that declining trees would show lower growth rates, smaller lumen areas (i.e., less theoretical hydraulic conductivity) and higher WUE_i than non-declining trees (Linares and Camarero 2012). Finally, $\delta^{18}O$ should increase in declining trees as compared with non-declining trees, indicating an enhanced stomatal control of water loss linked to canopy dieback (Scheidegger et al. 2000).

Materials and methods

Study sites

We selected two oak (*Q. frainetto* Ten.) forests showing recent dieback, located close to San Paolo Albanese (40°01′20′N, 16°20′46′E, 950 m above sea level (a.s.l.), mean slope 25–30%; hereafter SP site) and Oriolo (40°00′10″N, 16°23′30″E; 770 m a.s.l., mean slope 25%; hereafter OR site) villages, situated in the Basilicata and Calabria regions (southern Italy), respectively. The SP stand accounts for a density of 348 trees ha^{-1}, while average diameter at 1.3 m (d.b.h.) and age are 40 cm and 145 years, respectively. In the OR site, the mean d.b.h. and age are 35 cm

and 138 years, while mean density is 444 trees ha^{-1}. Both sites are located in high oak forests. The soil in both study sites is formed by sands and clays. No recent disturbance has been reported for the study sites (e.g., insect outbreaks or fires) and no silvicultural treatment has been applied in the last five decades.

The SP and OR study sites have shown dieback symptoms since the early 2000s (shoot dieback, leaf loss and withering, growth decline, high mortality). The densities of dead trees at the SP and OR sites are 35 stems ha^{-1} and 25 stems ha^{-1} (5%), respectively. The most affected areas encompass ca 250 and 600 ha in the SP and OR sites, respectively. The frequency of trees showing crown-transparency levels above the 50% threshold are 80% and 50% of trees in the SP and OR sites, respectively (see Figure S1 available as Supplementary Data at *Tree Physiology* Online). Therefore, we considered that the SP site was more affected by drought than the OR site. Further, given the unavailability of microclimate data for the two sites, we used the percentage of dead and defoliated trees as an indirect measure of drought impact.

Climate in the study areas is Mediterranean, characterized by dry and warm summers (mean June to August precipitation is 79 mm) and wet and mild winters (mean December to February precipitation is 257 mm) with a mean annual temperature of 16.4 °C and annual precipitation of 742 mm (data from Oriolo station, 40°03′11″N, 16°26′47″E, 445 m a.s.l., 1950–2015 period; see Figure S2 available as Supplementary Data at *Tree Physiology* Online). The warmest and coldest months are July (average maximum temperature of 33.5 °C) and January (average minimum temperature of 4.0 °C), respectively, whereas the driest and wettest months are July (22 mm) and December (99 mm). Drought occurs from June to September. Due to the shortness and heterogeneity of some local climate data, we used gridded (0.25° resolution) climate data from the E-OBS data set ver. 13.0 (Haylock et al. 2008) to quantify climate trends and climate–growth associations. Climate was extracted from the 0.25° grid with coordinates 40.00–40.25°N, 16.25–16.50°E. To evaluate drought–growth associations stress since 1950, we downloaded the Standardized Precipitation Evapotranspiration Index (SPEI) for the 0.5° grid where the study sites are located using the Global SPEI database webpage (http://sac.csic.es/spei/database.html). The SPEI is a multiscalar drought index, which considers the effects of temperature and evapotranspiration on drought severity and indicates wet (positive SPEI values) and dry (negative SPEI values) conditions (Vicente-Serrano et al. 2010).

Field sampling

First, seven circular plots (radius of 15 m) were randomly located in each of the SP and OR sites to describe the stand structure (density, basal area). Within each plot, dieback of all mature oak trees was characterized by a visual assessment of crown transparency made by two independent observations of the same tree (Dobbertin 2005, Camarero et al. 2016). Declining oaks (hereafter D trees) were considered those with crown transparency higher than 50%, whereas non-declining oaks (hereafter ND trees) were considered those with transparency lower than 50%. Using other crown-transparency thresholds (40% and 60%), the main results presented here did not change.

Tree-ring analyses

A total of 17 and 16 pairs of dominant and neighboring oak trees with contrasting vigor (ND–D couples) were selected at SP and OR sites in summer 2014 to estimate their growth trends using dendrochronology. Within each ND–D couple, trees were 10–15 m apart at maximum. Four wood cores from each tree were sampled at breast height (1.30 m) using a 5-mm Pressler increment borer. Two cores were used for tree-ring analyses and wood anatomy, another core was used for isotope analyses and the last core for NSCs analysis in the sapwood. A total of 34 and 32 trees were used for tree-ring width measurements at SP and OR study sites, respectively (Table 1). Quantitative wood anatomy was performed on a subsample of 10 cores from each considered site, i.e., five trees for each of the two vigor classes.

Wood samples were air-dried and the surface of the cores was cut using a sledge core microtome (Gärtner and Nievergelt 2010). Tree rings were visually cross-dated and measured with precision of 0.01 mm using a binocular microscope coupled to a computer with the LINTAB package (Rinntech, Heidelberg, Germany). The COFECHA program (Holmes 1983) was used to evaluate the visual cross-dating of tree-ring series. To quantify growth trends, we transformed the tree-ring widths into annual basal area increment (BAI) using the following formula:

$$BAI = \pi(R_t^2 - R_{t-1}^2), \quad (1)$$

Table 1. Characteristics of the non-declining (ND) and declining (D) Italian oak trees sampled in the two study sites (OR and SP). Values are means ± SE. Different letters indicate significant differences ($P < 0.05$; Mann–Whitney U tests) between tree types within each considered site.

Site	Tree type	No. of trees	D.b.h. (cm)	Height (m)	Age at 1.3 m (years)
SP	ND	17	31.9 ± 0.8b	11.3 ± 0.5b	142 ± 5a
	D	17	27.9 ± 1.0a	10.2 ± 0.3a	144 ± 4a
OR	ND	16	32.1 ± 0.6a	10.7 ± 0.3a	141 ± 4a
	D	16	30.0 ± 0.9a	10.1 ± 0.3a	140 ± 3a

where R is the radius of the tree and t is the year of tree-ring formation.

To quantify climate–growth relationships, first we removed the long-term trends of tree-ring width series by detrending them through Friedman's super smoother, which preserves high-frequency (yearly) variability in the resulting ring-width indices. In addition, an autoregressive model was applied to each detrended series to remove most of the first-order autocorrelation related to the previous year of growth. We obtained series at the tree level of dimensionless ring-width indices. Finally, a biweight robust mean was used to obtain mean chronologies of ND and D trees at each site. Chronology development and standardization were carried out using the ARSTAN program (Cook and Krusic 2005). Climate–growth associations were calculated for the 1950–80 period, i.e., prior to the dieback onset, considering monthly and seasonal climatic variables (mean maximum and minimum temperatures, precipitation). The window of analyses included from the previous October to current September based on previous studies (Tessier et al. 1994). Drought–growth associations were calculated for the same period using 1- to 20-month-long SPEI values obtained from January to December.

Wood anatomy

Wood anatomy was analyzed for the 1980–2013 period. The five trees of each vigor class used in these and further (isotopes, carbohydrates) analyses were selected based on the highest correlations of their ring-width series with the mean chronology of each tree class developed for each study site. Semi-thin transversal sections (20 μm) were obtained from one core per tree by dividing it into pieces of ~2 cm length. Sections were cut using a sliding microtome (Microm HM 400, Thermo Sci., Walldorf, Germany) and stained with safranin (1%) and astra-blue (2%), dehydrated with ethanol (70%, 95% and 100%) and xylol, and mounted on microscope slides using Eukitt® (Sigma-Aldrich, St Louis, MO, USA). Images were captured at ×20 and ×40 magnification using a transmitted light microscope (Zeiss Axiophot, Carl Zeiss Microscopy, Jena, Germany). Earlywood and LW vessels were analyzed in tangential windows of 2 and 0.3 mm, respectively. Earlywood vessels were considered those with lumen diameters larger than 50 μm. Vessel lumen diameter (along the radial direction) and area were measured using the ImageJ software (Schneider et al. 2012). We quantified the following wood-anatomical traits following Scholz et al. (2013): ring area, EW and LW areas, absolute and relative (%) areas occupied by vessels in the EW and LW, EW and LW vessel lumen area (mean, minimum and maximum values), and EW and LW vessel density. We also calculated two additional variables (*Dh*, hydraulic diameter; *Kh*, potential hydraulic conductivity) by weighting individual vessel lumen diameters to correspond to the average Hagen–Poiseuille lumen theoretical hydraulic conductivity for a vessel size (Tyree and Zimmermann 2002). The *Dh* was calculated as the average of $\Sigma d^5/\Sigma d^4$, where d is the lumen diameter of each vessel (Sperry et al. 1994). The *Kh* was estimated as $Kh = (\rho \times \pi \times \Sigma d^4)/(128 \times \mu \times Ar)$, where ρ is the density of water at 20 °C (998.2 kg m^{-3} at 20 °C), d is the vessel lumen diameter, μ is the viscosity of water (1.002×10^{-9} MPa s at 20 °C) and *Ar* is the area imaged (Tyree and Zimmermann 2002). The *Dh* and the *Kh* were calculated considering all EW and LW measured vessels. Finally, we obtained the vulnerability index (*VI*) following Carlquist (1977) by calculating the ratio between the mean vessel lumen diameter and vessel density. The *VI* is a proxy for the tree resistance to drought- or frost-induced cavitation with low ($VI < 1$) and high ($VI > 3$) values indicating xeromorphy and mesomorphy, respectively.

Non-structural carbohydrate concentrations in sapwood

The sapwood fraction of each core from the five trees selected in wood anatomy and isotope analyses was visually determined in the field and separated using a razor blade to determine the concentrations of NSCs. All sapwood samples were collected at the end of the growing season in 2015, transported to the laboratory in a portable cooler, and they were frozen and stored at −20 °C until freeze-dried. Then, they were weighed and milled to a fine powder in a ball mill (Retsch Mixer MM301, Leeds, UK). Soluble sugars were extracted with 80% (v/v) ethanol and their concentration determined colorimetrically using the phenol-sulfuric method (Buysse and Merckx 1993). Starch and complex sugars remaining after ethanol extraction were enzymatically digested with an enzyme mixture containing amyloglucosidase to reduce glucose as described in Palacio et al. (2007). Non-structural carbohydrates measured after ethanol extractions are referred to as SS, and carbohydrates measured after enzymatic digestion are referred to as starch. The NSC concentrations (% dry matter) were calculated as the sum of SS and starch concentrations.

Stable isotope analyses

The carbon and oxygen isotopes analysis was performed on the same trees used for wood-anatomical analyses (five ND trees plus five D trees per study site). We used rings spanning the period 1981–2013 to avoid a possible juvenile effect and focused on this most recent period where ND and D performance is expected to differ. Groups of three contiguous rings (e.g., 1981–83, … , 2011–13; $n = 11$ samples per tree) from the best five cross-dating trees per site were split using a scalpel and pooled together for each tree. These groups of rings were milled to a fine powder with a mixer mill (Retsch MM301, Haan, Germany). We then proceeded to extract α-cellulose on 10 mg of wood per group of three rings to remove extractives and lignin with a double-step digestion (Boettger et al. 2007, Battipaglia et al. 2008).

The carbon and oxygen stable isotope compositions were measured at the CIRCE Laboratory (Center for Isotopic Research on the Cultural and Environmental Heritage, Caserta, Italy) by continuous-flow isotope ratio mass spectrometry (Delta V plus Thermo electron corporation, Bremen Germany). We processed 1 mg of wood obtaining a cellulose yield of 50–60% using 0.06 mg for carbon isotope and 0.1–0.3 mg for oxygen isotope analysis.

Carbon isotope discrimination was used to account for the Suess effect (decrease in $\delta^{13}C$ of atmospheric CO_2 since the beginning of industrialization) resulting from the emission of fossil CO_2, which is depleted in ^{13}C (McCarroll and Loader 2004). Stable isotope ratios were expressed as per mil deviations using the δ notation relative to Vienna Pee Dee Belemnite and Vienna Standard Mean Ocean Water standards in the case of carbon and oxygen isotopes, respectively. The accuracy of the analyses (SD of working standards) was 0.06–0.20‰.

Calculation of WUE_i from carbon isotope ratios

We used the carbon isotopic ratio of tree-ring cellulose ($\delta^{13}C_{tree}$) to calculate WUE_i, i.e., the ratio between the photosynthetic rate (A) and its stomatal conductance (g). First, we calculated $\delta^{13}C_{tree}$ by using the following formula:

$$\delta^{13}C_{tree} = \delta^{13}C_{atm} - a - (b - a)\cdot\left(\frac{c_i}{c_a}\right), \quad (2)$$

where a is the fractionation factor due to CO_2 diffusion through stomata (4.4‰), b is the fractionation factor due to Rubisco enzyme during photosynthesis (27‰), and c_a and c_i represent the atmospheric (measured at the Mauna Loa station by NOAA) (http://www.esrl.noaa.gov) and the intercellular CO_2 concentrations, respectively (Farquhar et al. 1989). We used $\delta^{13}C_{atm}$ estimated values for the period 1960–2003 from McCarroll and Loader (2004) and Ferrio et al. (2005), and measured values for the 2004–2013 period available online (http://www.esrl.noaa.gov/gmd/). The $\delta^{13}C_{tree}$ values were obtained from tree-ring cellulose samples. Then, we derived c_i as follows:

$$c_i = c_a\left[\frac{(\Delta^{13}C - a)}{(b - a)}\right], \quad (3)$$

where the carbon isotope discrimination ($\Delta^{13}C$) represents the difference between the carbon isotopic ratio of atmospheric CO_2 ($\delta^{13}C_{air}$) and tree-ring cellulose ($\delta^{13}C_{tree}$) calculated as follows:

$$\Delta^{13}C = \frac{(\delta^{13}C_{air} - \delta^{13}C_{tree})}{(1 + \delta^{13}C_{tree})}. \quad (4)$$

Finally, the WUE_i can be calculated as follows:

$$WUE_i = \frac{(c_a - c_i)}{1.6} = \frac{A}{g}, \quad (5)$$

where 1.6 is the ratio of diffusivities of water and CO_2 in the atmosphere.

Statistical analyses

Trends in climatic variables were assessed using the Kendall τ statistic. To compare mean values of the analyzed variables (BAI, wood anatomy, NSCs, isotopes) between the two vigor classes at each site we used the Mann–Whitney U test. The relationships between growth, wood-anatomical traits and isotope data were evaluated using Pearson correlations. We used the Wilcoxon rank-sum test to check if the changes through time of BAI, wood-anatomical variables or isotope ratios differed between ND and D trees (Hentschel et al. 2014). We chose this non-parametric test because it is robust against deviations from standard distributions and the presence of temporal autocorrelation (Gibbons and Chakraborti 2011).

Results

Climate trends and droughts

We found a significant warming trend of minimum and maximum summer and spring temperatures at the study area since 1950 (see Figure S3 and Table S1 available as Supplementary Data at *Tree Physiology* Online). Dry conditions during the spring growing season occurred in several years (1957, 1975, 1977, 1992, 1995, 1999, 2001–02 and 2011–12; see Figure S3 available as Supplementary Data at *Tree Physiology* Online). The 10-month-long May SPEI, which captures drought severity during the growing season, detected severe droughts in 1957, 1995, 2000, 2002 and 2013 (Figure S4 available as Supplementary Data at *Tree Physiology* Online).

Size, growth and climate–growth associations

The D trees presented thinner and shorter stems than ND trees at the most affected SP site (Table 1). At this site, ND tree-ring growth was higher in some past period (1930s) than D trees, but the reverse pattern was observed at the OR site during the wet 1960s and 1970s decades (Figure 1).

The D trees displayed a sharp growth drop after the onset decline comparing with ND trees, with reductions of 49% and 44% at sites SP and OR, respectively. Further, we found that D trees showed significantly lower BAI values than ND trees after 2002 and 2009 at the SP and OR study sites, respectively (Figure 1). Considering only the 1980–2013 period, when growth, wood anatomy and isotope data were available, BAI showed significantly ($P < 0.05$) higher values in ND than D trees at both study sites (SP, 3.1 ± 0.2 cm^2 vs 2.2 ± 0.1 cm^2; OR, 3.0 ± 0.2 cm^2 vs 2.5 ± 0.1 cm^2; Figure 1).

The D trees from the most affected SP site were the most sensitive to drought stress in terms of growth reduction (Figure S5 available as Supplementary Data at *Tree Physiology* Online). At both study sites, D trees showed more growth enhancement in

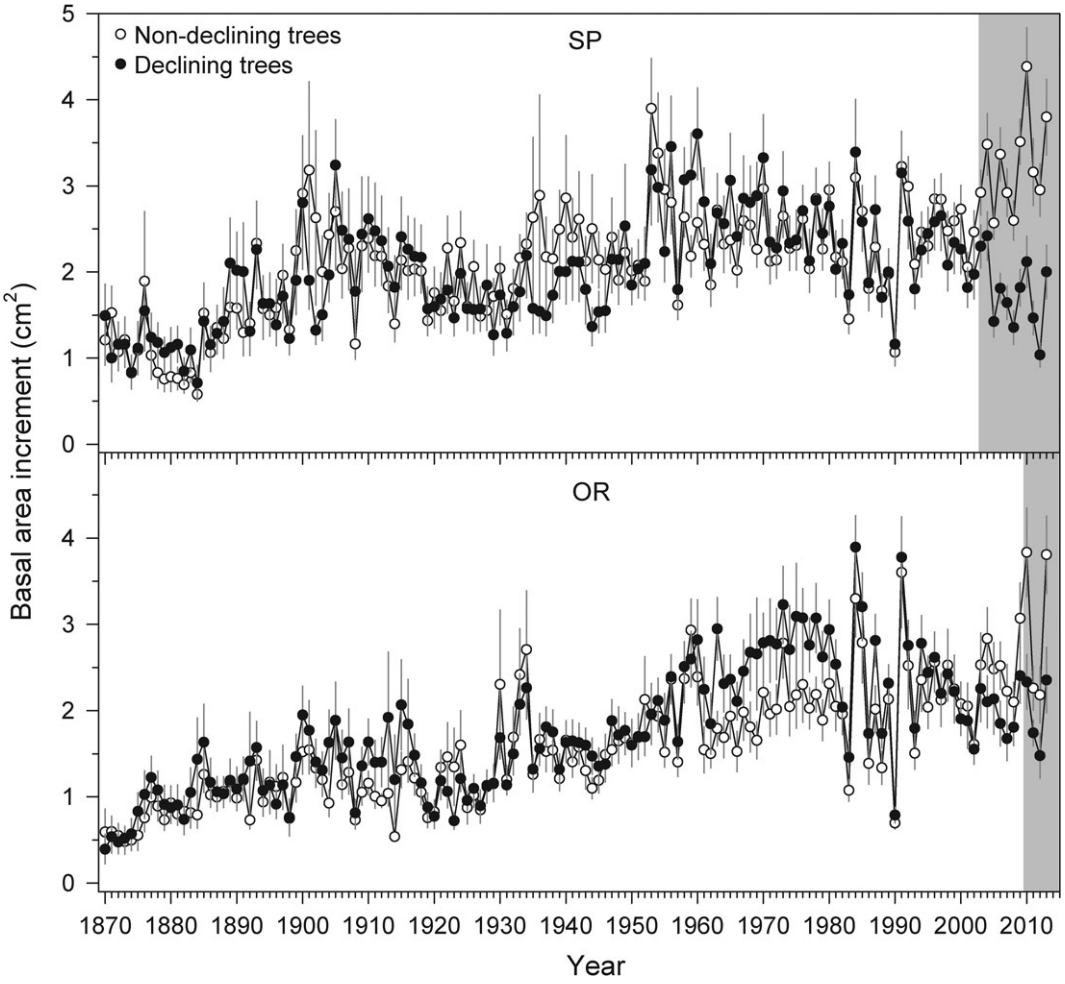

Figure 1. Growth trends (BAI) of non-declining (empty symbols) and declining (filled symbols) oak trees in the two study sites (SP and OR) from southern Italy. Values are means ± SE. The gray filled areas indicate the period when BAI of D and ND trees significantly ($P < 0.05$) differed.

response to cool and wet spring conditions than ND trees. Differences between ND and D trees were found for correlations of growth indices with May precipitation (SP site, ND trees, $r = 0.20 \pm 0.03$, D trees, $r = 0.32 \pm 0.05$; OR site, ND trees, $r = 0.19 \pm 0.03$, D trees, $r = 0.28 \pm 0.04$) and for spring mean maximum temperatures (SP site, ND trees, $r = -0.32 \pm 0.03$, D trees, $r = -0.41 \pm 0.04$; OR site, ND trees, $r = -0.27 \pm 0.03$, D trees, $r = -0.35 \pm 0.04$). Consequently, the D trees from SP site showed the highest SPEI–growth correlation, specifically when considering spring months (May and June) and 2- to 10-month-long scales (Figure S6 available as Supplementary Data at *Tree Physiology* Online).

Wood anatomy

The D trees formed narrower EW vessels than ND from 2005 onwards and in 2012–13 at the SP and OR sites, respectively, while D trees at the SP site showed a higher LW area occupied by vessels in 2012–13 (Figure 2). In both sites, LW vessels tended to be larger in D than in ND trees, although these differences were not significant (Figure 2).

In agreement with the narrower EW vessel lumen area of D trees at the SP site, the *Dh* and the *Kh* were lower in D trees compared with ND trees but differences were significant only at the SP site (Table 2).

Non-structural carbohydrate concentrations in sapwood

We did not find any significant differences in SS, starch, NSC sapwood concentrations between ND and D trees either at the SP or at the OR site (Table 3). Interestingly, the NSC sapwood concentrations at the most drought affected SP site were significantly lower than at the least affected OR site ($U = 46$, $P = 0.0005$) due to differences between sites regarding SS ($U = 39$, $P = 0.0002$) but not starch concentrations ($U = 135$, $P = 0.5194$).

Carbon and oxygen isotopes in tree rings

Considering the 1980–2013 period, the isotope variables ($\delta^{13}C$, $\delta^{18}O$, WUE_i) showed no significant differences between

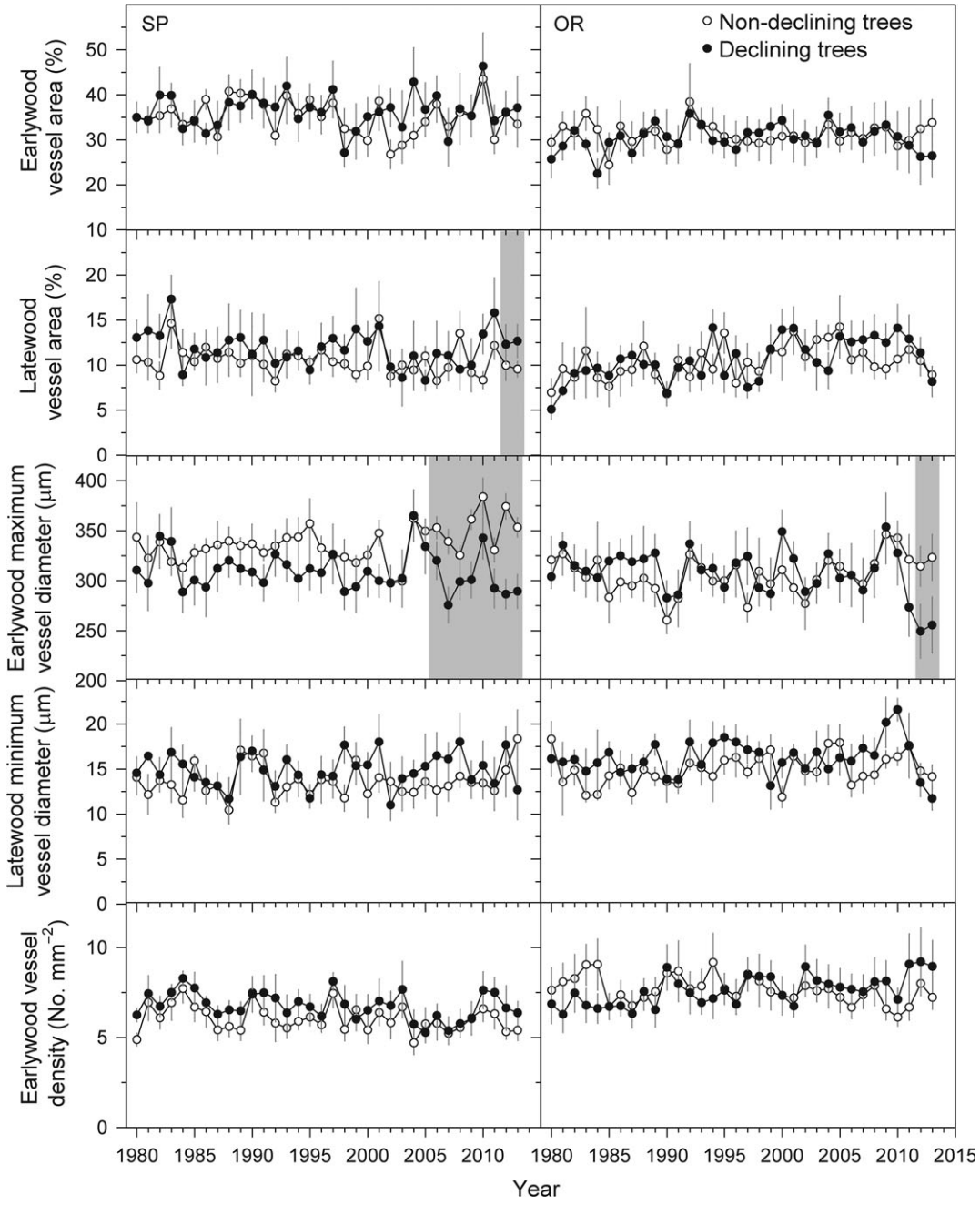

Figure 2. Wood-anatomical traits measured in non-declining (empty symbols) and declining (filled symbols) Italian oak trees in the two study sites (SP and OR). The gray filled areas indicate periods when the variables significantly ($P < 0.05$) differ between D and ND trees according to Wilcoxon tests. Values are means ± SE and correspond to the 1980–2013 period.

ND and D trees (Figures 3 and 4), while during the 2008–13 period when dieback intensified (i.e., when the difference in growth between ND and D trees was the highest), ND trees showed higher $\delta^{13}C$ values than D trees at the SP site (Figure 3). At the OR site, this occurred in the last analyzed period (2011–13). Similarly, the ND trees from the SP site showed higher WUE_i values than D trees during the 2008–13 period, whereas at the OR site WUE_i differenced only during the last period, 2011–13. After the dieback onset, reductions of WUE_i in D compared with ND trees were 9.7% and 5.6% at sites SP and OR, respectively. Warm spring and early summer conditions were related to high WUE_i values and dry conditions were associated with low $\delta^{18}O$ values (Table S2 available as Supplementary Data at *Tree Physiology* Online). The comparison of $\delta^{13}C$ and $\delta^{18}O$ values suggests a reduction of stomatal control of water loss in D trees (Figure 4).

Table 2. Wood-anatomical variables obtained for non-declining (ND) and declining (D) Italian oak trees in the two study sites (SP and OR). The data correspond to the 1980–2013 period and are presented as mean ± SE. Abbreviations: *Dh*, hydraulic diameter; *Kh*, potential hydraulic conductivity; *Vl*, vulnerability index (ratio between mean vessel diameter and vessel density). Different letters indicate significant differences (for $P < 0.05$) between ND and D trees within each site (Mann–Whitney *U* tests).

Site	Tree type	No. of measured vessels	*Dh* (μm)	*Kh* (kg m^{-1} MPa^{-1} s^{-1}) × 10^{-2}	Earlywood			*Vl* (μm mm^{-2})	Latewood			
					Vessel diameter (μm)	Vessel area (%)	Vessel density (no. mm^{-2})		Vessel lumen diameter (μm)	Vessel area (%)	Vessel density (no. mm^{-2})	*Vl* (μm mm^{-2})
SP	ND	3501	331.6 ± 3.6b	85.7 ± 6.2b	248.8 ± 2.8a	35.3 ± 1.0a	6 ± 1a	41.5 ± 2.7a	24.4 ± 0.6a	10.3 ± 0.4a	22 ± 2a	1.2 ± 0.2b
	D	4063	321.2 ± 2.8a	66.9 ± 3.5a	246.5 ± 4.3a	35.6 ± 1.5a	6 ± 1a	41.1 ± 3.0a	26.1 ± 0.7a	12.0 ± 0.8b	37 ± 4b	0.6 ± 0.1a
OR	ND	4125	311.2 ± 1.6a	50.6 ± 4.4a	231.2 ± 5.1a	31.9 ± 1.3a	7 ± 1a	33.0 ± 4.5a	26.8 ± 0.7a	10.6 ± 0.6a	19 ± 1a	1.4 ± 0.5a
	D	4194	309.4 ± 1.2a	47.4 ± 4.1a	230.0 ± 5.7a	30.6 ± 1.0a	7 ± 1a	32.9 ± 4.8a	27.0 ± 0.8a	10.6 ± 0.5a	19 ± 1a	1.4 ± 0.4a

Table 3. Concentrations of NSCs in the sapwood of non-declining (ND) and declining (D) Italian oak trees sampled at the SP and OR study sites. Values are means ± SE. Different letters indicated significant differences ($P < 0.05$; Mann–Whitney *U* tests) between tree types within each site.

Site	Tree type	SS (%)	Starch (%)	NSC (%)
SP	ND	1.45 ± 0.15a	2.03 ± 0.19a	3.48 ± 0.23a
	D	1.41 ± 0.15a	1.73 ± 0.16a	3.14 ± 0.15a
OR	ND	2.09 ± 0.31a	2.24 ± 0.21a	4.33 ± 0.45a
	D	2.95 ± 0.41a	1.94 ± 0.29a	4.89 ± 0.39a

Associations between growth, wood anatomy and isotopes

We found a positive association between *Dh* and WUE_i in the case of ND trees at the site level (Figure 5). BAI and WUE_i were also significantly related in ND trees (Figure S7 available as Supplementary Data at *Tree Physiology* Online). Finally, we found that the mean LW vessel diameter and the $\delta^{18}O$ of ring cellulose were positively related at the OR site, but this association was negative in the case of ND trees from the SP site (Figure 6).

Discussion

The very warm and dry spring–summer conditions of the 1990s and 2000s triggered dieback of Italian oaks characterized by leaf shedding, shoot dieback and growth decline, which was particularly evident at the most affected site SP (Figure 1, and Figure S1 available as Supplementary Data at *Tree Physiology* Online). These climatic conditions have been shown to cause a reduction of growth in other deciduous oak species growing at Mediterranean drought-prone sites (Tessier et al. 1994). In the present study, declining and non-declining trees did not show differences in growth rate and vessel lumen area prior to the 2000s dieback episodes (Figures 1 and 2). Only during wet decades such as the 1970s, declining trees tended to show higher BAI values, but this occurred only at the OR site, which was less affected by drought. This is in contrast to other studies where physiological differences were found between declining and non-declining trees prior to dieback in oaks (Levanič et al. 2011) and conifers (Voltas et al. 2013). Therefore, our findings do not support a predisposition of the most affected trees in terms of wood anatomy, i.e., declining trees would produce wider conduits but more susceptible to drought-induced cavitation. The smaller size (d.b.h., height) of declining trees from the SP site does not indicate that the most susceptible trees to drought stress should support more leaf biomass, which could involve higher respiration costs (Levanič et al. 2011). Oaks display multiple structural strategies of drought resistance including adjustments of the ratio of leaf area to sapwood area or changes in the root system and xylem anatomy (Bréda et al. 2006, Klein et al. 2014). Other drought-avoidance strategies include partial or premature leaf shedding (this study and Peguero-Pina et al. 2015) or water storage in sapwood (Meinzer et al. 2003). More insight on oak dieback could be gained by quantifying

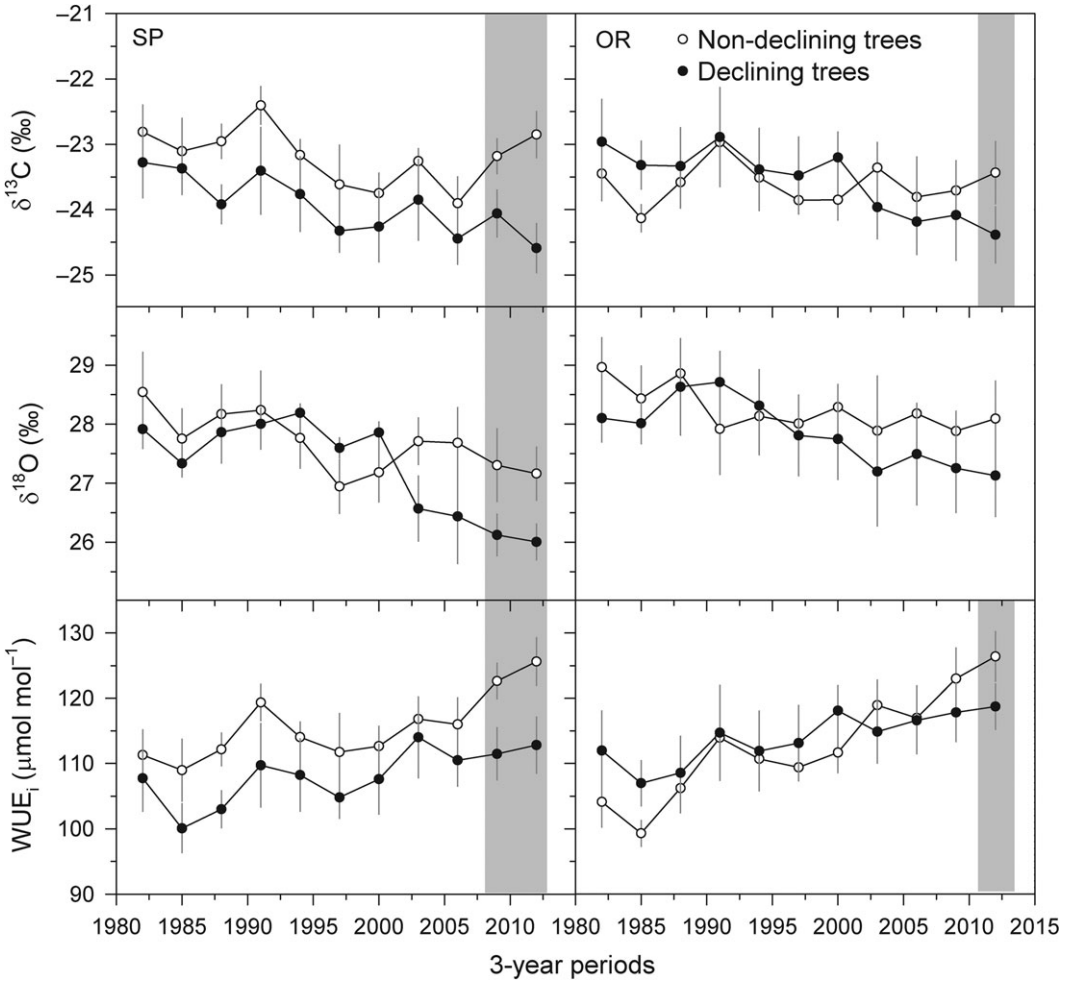

Figure 3. Trends in carbon ($\delta^{13}C$) and oxygen ($\delta^{18}O$) isotope ratios of tree-ring wood and WUE_i of non-declining (empty symbols) and declining (filled symbols) Italian oak trees sampled in the two study sites (SP and OR). The gray filled areas indicate periods when the variables significantly ($P < 0.05$) differ between D and ND trees according to Wilcoxon tests. Values correspond to means ± SE for 3-year ring segments ($n = 11$ samples per tree, $n = 5$ trees per site).

biomass allocation as related to microsite conditions (slope, soil depth and texture) of declining trees, since oak mortality may be also associated with impaired root systems (Thomas and Hartmann 1996). This approach could also consider genetic information (e.g., Lloret and García 2016) since we still lack data to explain why in neighboring trees subjected to similar climate conditions, some are more vulnerable to drought stress than others.

As expected, the sharp drop in growth rates of declining trees started in the late 2000s (Figure 1). This recent decline in growth was accompanied by changes in some wood-anatomical traits such as the reduction of EW vessel lumen area (Figure 2). Concurrently, the decrease of $\delta^{13}C$ and $\delta^{18}O$ in declining trees also happened during that period when dieback intensified (2008–13). These drops in growth and alterations in wood anatomy were most patent in the more affected SP site (Figures 1–3). It is also possible that the growth increase observed for non-declining trees at the OR site is the consequence of reduced competition for water and nutrients with the coexisting declining and dying trees. The decrease in $\delta^{13}C$ and $\delta^{18}O$ in declining trees as compared with non-declining trees (Figure 4) would correspond to increased stomatal conductance (g) according to Scheidegger et al. (2000), and agrees with the recent reduction of WUE_i in the declining trees, which was again more notable in the SP site (Figure 3). This is strictly linked with canopy dieback and with a less tight stomatal control of transpiration, perhaps as a mechanism to compensate drought stress, whereas carbon uptake through photosynthesis (A) remains stable.

Considering wood anatomy, we detected minor differences between vigor classes, suggesting a low plasticity of xylem traits as compared with leaf physiological features in response to drought. Perhaps, different functional thresholds exist regarding the detection of xylem (wood anatomy) and leaf (photosynthesis) responses to drought stress. Our findings agree with observations from a 6-year-long partial throughfall, where the evergreen diffuse-porous *Quercus ilex* responded to the induced drought by reducing leaf transpiring area and

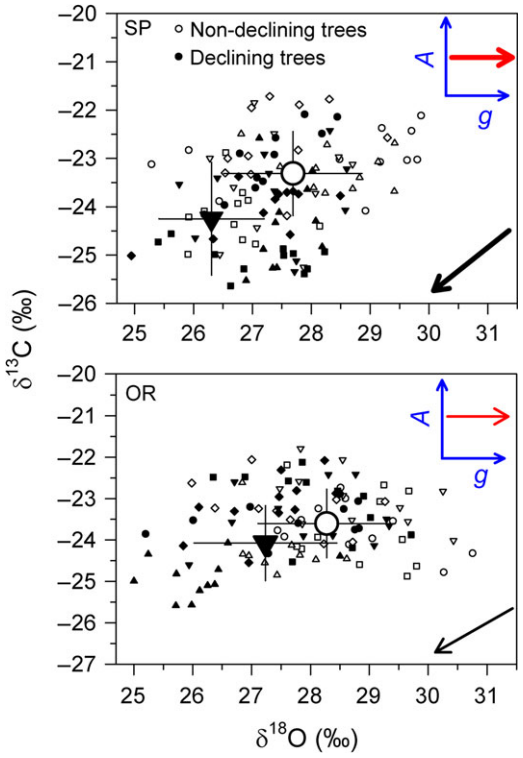

Figure 4. Scatter plots showing the associations between carbon ($\delta^{13}C$) and oxygen ($\delta^{18}O$) isotope ratios considering non-declining (empty symbols) and declining (filled symbols) oak trees at the SP and OR sites. The black arrows show the major trends of mean values of $\delta^{18}O$ and $\delta^{13}C$ comparing non-declining vs declining trees (small and big symbols show individual and mean ± SD values, respectively), whereas the insets indicate the inferred changes of stomatal conductance (*g*) vs photosynthesis rates (*A*). Data correspond to 3-year ring segments for the 1981–2013 period.

increasing leaf-specific conductivity, whereas vessel diameter and density remained largely unaffected albeit vessel lumen fraction (i.e., ratio between mean vessel lumen area and number per unit area) increased (Limousin et al. 2010). Contrastingly, drought reduced the lumen area of EW vessels in the ring-porous *Quercus pubescens*, thus lowering the hydraulic conductivity and reducing the risk of cavitation (Eilmann et al. 2009). This was consistent with our data from the declining trees at the SP site, where the production of smaller EW vessels by declining trees would explain their smaller hydraulic diameter and potential hydraulic conductivity (Figure 2). Others reported declines in vessel diameter as water availability decreases (Villar-Salvador et al. 1997) or in response to an extreme drought (Corcuera et al. 2004*a*), which can be consequent to reduced turgor-driven cell enlargement during xylogenesis. Overall, water shortage during spring and summer causes a severe reduction of LW production in ring-porous oaks species (Alla and Camarero 2012), which might increase their susceptibility to further water deficit if some EW vessels lose functionality due to cold- (Cavender-Bares and Holbrook 2001) and drought-induced cavitation in late winter and spring (Corcuera et al. 2004*b*, 2006). This could explain the trend toward forming wider LW vessels (Figure 2) and the consequent significant decrease of the vulnerability index in declining trees at the SP site (Table 2). The tendency to form LW vessels with lower minimum diameters in ND than D trees would guarantee continuous, although slow, water flow in the former under conditions promoting embolism.

We found no support to the carbon limitation hypothesis because sapwood NSC levels did not differ between declining and non-declining trees, but NSC and SS decreased in the most affected SP site (Table 3). According to Hoch (2015), hydraulic failure and growth cessation precede carbon starvation in most studies on drought-induced dieback. For instance, a seasonal study of NSC dynamics in *Quercus petraea* found that stem growth ceased when soil water content was depleted but the accumulation of NSCs was not affected and continued (Barbaroux and Bréda 2002). Sapwood NSCs can be too coarse a variable to test carbon starvation, which may be restricted to organs such as roots located away from leaves, thus suggesting hydraulic constraints on the transport of photoassimilates (Sala et al. 2010). The finding that NSC levels decreased in the most affected SP site as compared with the less affected OR site suggests that drought (e.g., the reduced spring precipitation observed in the early 2000s with 35–62% of the 1950–2015 mean record corresponding to −1.7 to −2.0 SPEI values) can constrain carbon storage to some level, but this threshold seems not to be as lethal as has been observed in another Mediterranean oak species (*Quercus faginea*) that experienced drought-induced dieback (Camarero et al. 2016). Our results do not exclude the involvement of carbon starvation in the studied drought-induced dieback episode since trees were exposed to prolonged water shortage, which could constrain carbon uptake due to stomatal limitation (Ogasa et al. 2013). However, hydraulic failure seems to be the most plausible cause of dieback as it has been observed under experimental conditions, where trees experienced extensive cavitation during advanced drought (Barigah et al. 2013, Hartmann et al. 2013).

Regarding isotope data, our results partially agree with those presented by Hentschel et al. (2014), who reported lower $\delta^{13}C$ values in declining *Picea abies* trees and interpreted them as an increase of stomatal conductance rates, while non-declining trees had low stomatal conductance, allowing them to prevent water loss during dry periods. The higher $\delta^{13}C$ of non-declining trees from the SP site (Figure 3) indicates an overall more conservative water use (Scheidegger et al. 2000) in comparison with declining individuals, suggesting the capacity of those individuals to effectively close stomata to prevent excessive water loss. In contrast, the dual-isotope approach allowed inferring a sustained increase of stomatal conductance in declining trees, probably leading to a positive feedback characterized by a drought- and heat-enhanced water loss through transpiration that is not compensated by reduced growth rates, smaller EW lumen areas and steady WUE_i (Ponton et al. 2001). This cascade of altered functioning would explain the uncoupling

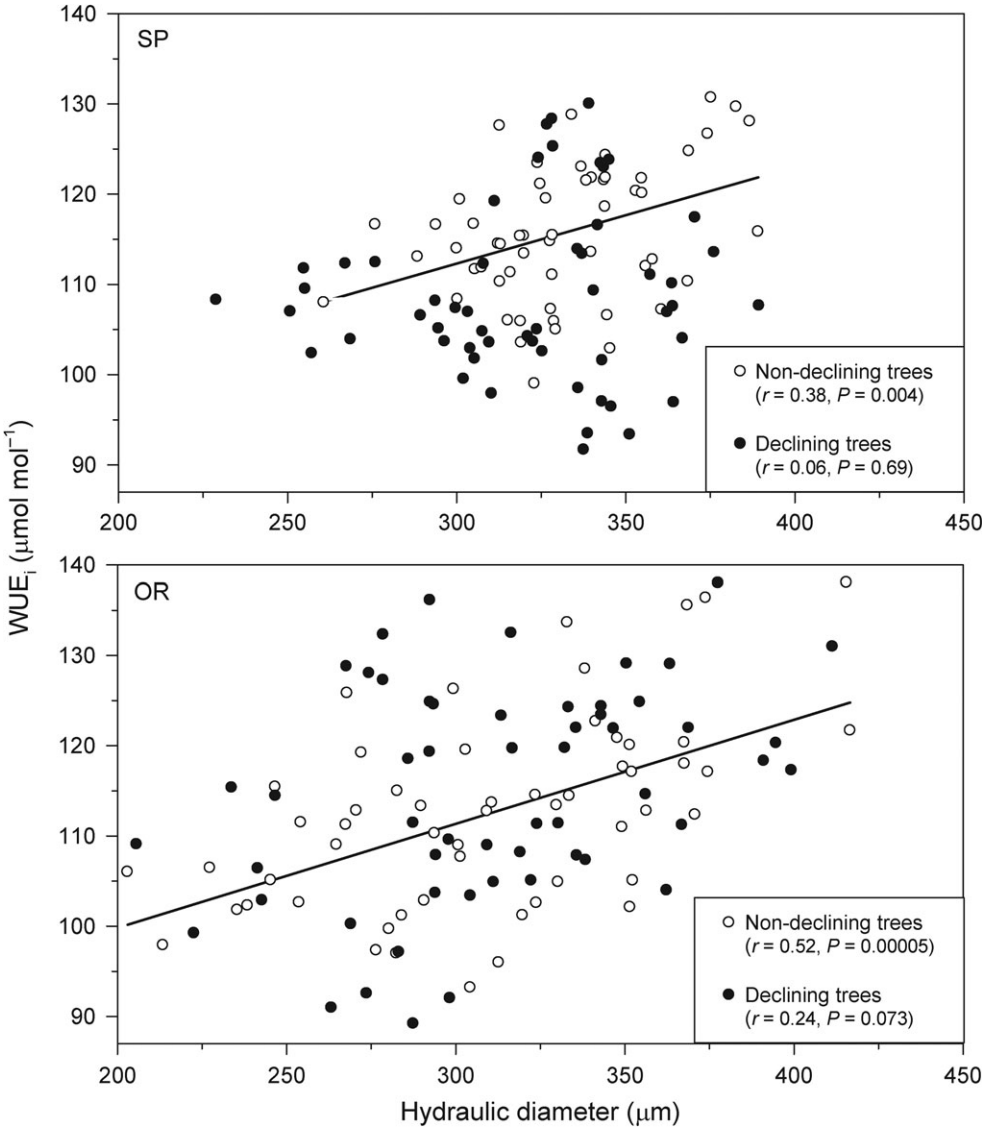

Figure 5. Diverse relationships observed between the hydraulic diameter and the WUE_i for non-declining (empty symbols) and declining (filled symbols) Italian oak trees at the two study sites (SP and OR). The continuous lines highlight the significant ($P < 0.05$) associations for non-declining trees (correlation statistics are shown for each tree type).

between growth and WUE_i in declining trees (Figure S7 available as Supplementary Data at *Tree Physiology* Online) and the lack of association observed at the most affected SP site between LW vessel lumen diameter, a proxy for summer hydraulic conductivity, and $\delta^{18}O$, a proxy for evaporative demand (Figure 6). It may be also the case that the drought-induced sharp reduction of growth uncouples the tree-ring and leaf isotope signatures (Pflug et al. 2015), thus making the dual-isotope approach unreliable (Roden and Siegwolf 2012).

Finally, the study forests have not been recently managed, but their previous management during early stand development may have shaped their current stand structure (e.g., stand density, hydraulic architecture and height of trees), which could influence the recent tree responses to droughts. Stand density reductions could improve the water balance of these forests (McDowell et al. 2006), but currently they are not dense forests. More importantly, the fact that anysohydric species with ring-porous wood such as the Italian oak succumb to warm and severe dry conditions questions the validity of thinning once VPD has reached such minimum values that stomatal conductance reaches very low values and xylem cavitation becomes widespread.

Conclusions

Although a further advance in the knowledge has been achieved from the plethora of recent studies on drought-induced dieback, this process remains a poorly understood phenomenon. The main reason is that the comprehension of causes and mechanisms

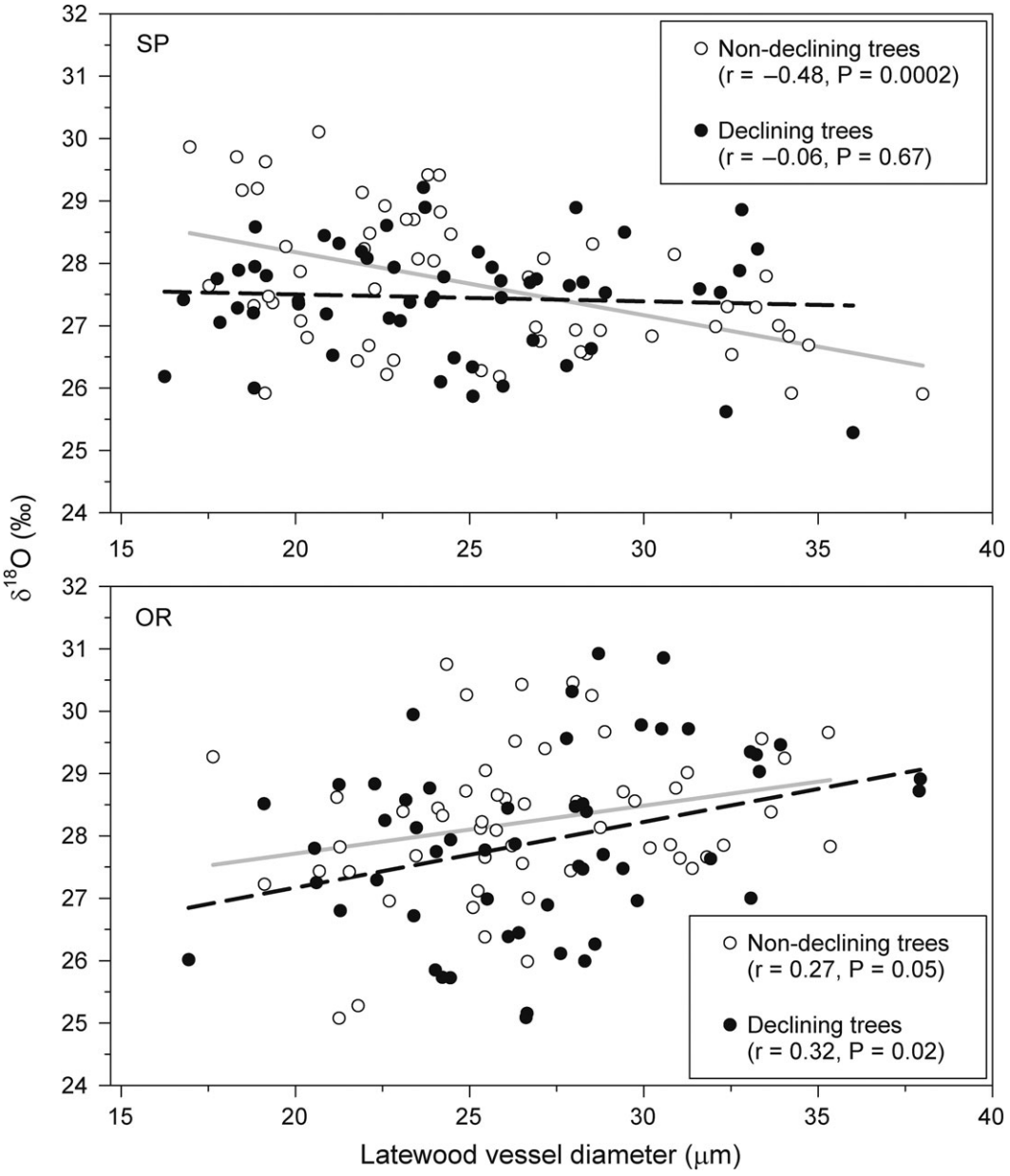

Figure 6. Contrasting relationships observed between the mean LW vessel diameter and the wood oxygen isotope ratio ($\delta^{18}O$) for the non-declining (empty symbols) and declining (filled symbols) Italian oak trees sampled at the SP and OR study sites. Continuous and dashed lines show these associations for non-declining and declining trees, respectively (correlation statistics are shown for each tree type). Data correspond to the 1980–2013 period.

involved necessarily requires a multi-proxy approach, which is often lacking from studies. Our approach, by investigating on either physiological or structural aspects, partially supports hydraulic failure as the potential cause of oak dieback. We observed that declining tress presented a reduced WUE_i after the onset of dieback, especially in the most drought-affected site, which is coherent with an enhanced water loss. These joint evidences, with the parallel absence of any significant differences in sapwood NSC concentrations, partially support the hydraulic failure mechanism of dieback. In future scenarios of increased severity and duration of droughts, as foreseen under warmer conditions, dieback phenomena may affect drought-tolerant anysohydric species, as they keep a narrow margin of hydraulic safety.

Supplementary Data

Supplementary Data for this article are available at *Tree Physiology* Online.

Acknowledgments

We acknowledge the E-OBS data set from the EU-FP6 project ENSEMBLES (http://ensembles-eu.metoffice.com) and the data providers in the ECA&D project (http://www.ecad.eu).

Conflict of interest

None declared.

Funding

This research was financially supported by the project 'Alarm of forest mortality in Southern Italy' (Gorgoglione Administration, Basilicata Region, Italy) and by the CGL2015–69186-C2-1-R project (Spanish Ministry of Economy). M.C. was supported by the PhD program from the course of Agricultural, Forest and Food Science at the University of Basilicata (Italy).

References

Alla AQ, Camarero JJ (2012) Contrasting responses of radial growth and wood anatomy to climate in a Mediterranean ring-porous oak: implications for its future persistence or why the variance matters more than the mean. Eur J For Res 131:1537–1550.

Allen CD, Macalady AK, Chenchouni H et al. (2010) A global overview of drought and heat-induced tree mortality reveals emerging climate change risks for forests. For Ecol Manage 259:660–684.

Attia Z, Domec J-C, Oren R, Way DA, Moshelion M (2015) Growth and physiological responses of isohydric and anisohydric poplars to drought. J Exp Bot 66:4373–4381.

Barbaroux C, Bréda N (2002) Contrasting distribution and seasonal dynamics of carbohydrate reserves in stem wood of adult ring-porous sessile oak and diffuse-porous beech trees. Tree Physiol 22: 1201–1210.

Barbour MM, Walcroft AS, Farquhar GD (2002) Seasonal variation in $\delta^{13}C$ and $\delta^{18}O$ of cellulose from growth rings of *Pinus radiata*. Plant Cell Environ 25:1483–1499.

Barigah TS, Charrier O, Douris M, Bonhomme M, Herbette S, Améglio T, Fichot R, Brignolas F, Cochard H (2013) Water stress-induced xylem hydraulic failure is a causal factor of tree mortality in beech and poplar. Ann Bot 112:1431–1437.

Battipaglia G, Jäggi M, Saurer M, Siegwolf RTW, Cotrufo MF (2008) Climatic sensitivity of $\delta^{18}O$ in the wood and cellulose of tree rings: results from a mixed stand of *Acer pseudoplatanus* L. and *Fagus sylvatica*. Palaeogeogr Palaeoclimatol Palaeoecol 261:193–202.

Battipaglia G, De Micco V, Brand WA, Linke P, Aronne G, Saurer M, Cherubini P (2010) Variations of vessel diameter and $\delta^{13}C$ in false rings of *Arbutus unedo* L. reflect different environmental conditions. New Phytol 188:1099–1112.

Billings SA, Boone AS, Stephen FM (2016) Tree-ring $\delta^{13}C$ and $\delta^{18}O$, leaf $\delta^{13}C$ and wood and leaf N status demonstrate tree growth strategies and predict susceptibility to disturbance. Tree Physiol 36: 576–588.

Boettger T, Haupt M, Knöller K et al. (2007) Wood cellulose preparation methods and mass spectrometric analyses of $\delta^{13}C$, $\delta^{18}O$, and nonexchangeable $\delta^{2}H$ values in cellulose, sugar, and starch: an interlaboratory comparison. Anal Chem 79:4603–4612.

Bréda N, Huc R, Granier A, Dreyer E (2006) Temperate forest trees and stands under severe drought: a review of ecophysiological responses, adaptation processes and long-term consequences. Ann For Sci 63: 625–644.

Buysse J, Merckx R (1993) An improved colorimetric method to quantify sugar content of plant tissue. J Exp Bot 44:1627–1629.

Camarero JJ, Sangüesa-Barreda G, Vergarechea M (2016) Prior height, growth, and wood anatomy differently predispose to drought-induced dieback in two Mediterranean oak species. Ann For Sci 73:341–351.

Carlquist S (1977) Ecological factors in wood evolution: a floristic approach. Am J Bot 64:887–896.

Cavender-Bares J, Holbrook NM (2001) Hydraulic properties and freezing-induced cavitation in sympatric evergreen and deciduous oaks with contrasting habitats. Plant Cell Environ 24:1243–1256.

Chatziphilippidis G, Spyroglou G (2004) Sustainable management of coppice forests in Greece. Towards the sustainable use of Europe's forests—Forest Ecosystem and Landscape Research: Scientific Challenges and Opportunities. In: Andersson F, Birot Y, Paivinen R (eds) EFI Proceedings 49, European Forest Institute, Joensuu, Finland, pp 51–60.

Cook ER, Krusic PJ (2005) Program ARSTAN: A tree-ring standardization program based on detrending and autoregressive time series modeling, with interactive graphics. Columbia University, Palisades, New York, NY.

Corcuera L, Camarero JJ, Gil-Pelegrin E (2004*a*) Effects of a severe drought on *Quercus ilex* radial growth and xylem anatomy. Trees 18: 83–92.

Corcuera L, Camarero JJ, Gil-Pelegrín E (2004*b*) Effects of a severe drought on growth and wood-anatomical properties of *Quercus faginea*. IAWA J 25:185–204.

Corcuera L, Camarero JJ, Sisó S, Gil-Pelegrín E (2006) Radial-growth and wood-anatomical changes in overaged *Quercus pyrenaica* coppice stands: functional responses in a new Mediterranean landscape. Trees 20:91–98.

Dobbertin M (2005) Tree growth as indicator of tree vitality and of tree reaction to environmental stresses: a review. Eur J For Res 124: 319–333.

Drobyshev I, Linderson H, Sonesson K (2007) Temporal mortality pattern of pedunculate oaks in southern Sweden. Dendrochronologia 24: 97–108.

Dwyer JP, Cutter BE, Wetteroff JJ (1995) A dendrochronological study of black and scarlet oak decline in the Missouri Ozarks. For Ecol Manage 75:69–75.

Eilmann B, Zweifel R, Buchmann N, Fonti P, Rigling A (2009) Drought-induced adaptation of the xylem in Scots pine and pubescent oak. Tree Physiol 29:1011–1020.

Farquhar GD, Ehleringer J, Hubick K (1989) Carbon isotope discrimination and photosynthesis. Ann Rev Plant Phys 40:503–537.

Ferrio JP, Voltas J (2005) Carbon and oxygen isotope ratios in wood constituents of *Pinus halepensis* as indicators of precipitation, temperature and vapour pressure deficit. Tellus B 57:164–173.

Ferrio JP, Araus JL, Buxó R, Voltas J, Bort J (2005) Water management practices and climate in ancient agriculture: inferences from the stable isotope composition of archaeobotanical remains. Veg Hist Archaeobot 14:510–517.

Gärtner H, Nievergelt D (2010) The core-microtome: a new tool for surface preparation on cores and time series analysis of varying cell parameters. Dendrochronologia 28:85–92.

Gea-Izquierdo G, Viguera B, Cabrera M, Cañellas I (2014) Drought induced decline could portend widespread pine mortality at the xeric ecotone in managed Mediterranean pine-oak woodlands. For Ecol Manage 320:70–82.

Gibbons JD, Chakraborti S (2011) Nonparametric statistical inference, 5th ed. CRC Press, New York, NY.

Haavik LJ, Stahle DW, Stephen FM (2011) Temporal aspects of *Quercus rubra* decline and relationship to climate in the Ozark and Ouachita Mountains, Arkansas. Can J Forest Res 41:773–781.

Hacke UG, Sperry JS, Pockman WT, Davis SD, McCulloh KA (2001) Trends in wood density and structure are linked to prevention of xylem implosion by negative pressure. Oecologia 126:457–461.

Hartmann H, Ziegler W, Kolle O, Trumbore S (2013) Thirst beats hunger —declining hydration during drought prevents carbon starvation in Norway spruce saplings. New Phytol 200:340–349.

Haylock MR, Hofstra N, Klein Tank AMG, Klok EJ, Jones PD, New M (2008) A European daily high-resolution gridded dataset of surface

temperature and precipitation. J Geophy Res (Atmospheres) 113: D20119.
Hentschel R, Rosner S, Kayler ZE, Andreassen K, Børja I, Solverg S, Tveito OE, Priescak E, Gessler A (2014) Norway spruce physiological and anatomical predisposition to dieback. For Ecol Manage 322: 27–36.
Hoch G (2015) Carbon reserves as indicators for carbon limitation in trees. Prog Bot 76:321–346.
Hoffmann WA, Marchin RM, Abit P, Lau OL (2011) Hydraulic failure and tree dieback are associated with high wood density in a temperate forest under extreme drought. Glob Chang Biol 17:2731–2742.
Holmes RL (1983) Computer-assisted quality control in tree-ring dating and measurement. Tree-Ring Res 43:69–78.
Hsiao TC (1973) Plant responses to water stress. Annu Rev Plant Physiol 24:519–570.
Klein T (2014) The variability of stomatal sensitivity to leaf water potential across tree species indicates a continuum between isohydric and anisohydric behaviours. Funct Ecol 28:1313–1320.
Klein T, Yakir D, Buchmann N, Grünzweig JM (2014) Towards an advanced assessment of the hydrological vulnerability of forests to climate change-induced drought. New Phytol 201:712–716.
Levanič T, Cater M, McDowell NG (2011) Associations between growth, wood anatomy, carbon isotope discrimination and mortality in a *Quercus robur* forest. Tree Physiol 31:298–308.
Limousin JM, Longepierre D, Huc R, Rambal S (2010) Change in hydraulic traits of Mediterranean *Quercus ilex* subjected to long-term throughfall exclusion. Tree Physiol 30:1026–1036.
Linares JC, Camarero JJ (2012) From pattern to process: linking water-use efficiency to drought-induced forest decline. Glob Chang Biol 18: 1000–1015.
Lloret F, García C (2016) Inbreeding and neighbouring vegetation drive drought-induced die-off within juniper populations. Funct Ecol. 30: 1696–1704.
McCarroll D, Loader NJ (2004) Stable isotopes in tree rings. Quat Sci Rev 23:771–801.
McDowell NG (2011) Mechanisms linking drought, hydraulics, carbon metabolism, and vegetation mortality. Plant Physiol 155:1051–1059.
McDowell NG, Allen CD (2015) Darcy's law predicts widespread forest mortality under climate warming. Nat Clim Change 5:669–672.
McDowell NG, Adams HD, Bailey JD, Hess M, Kolb TE (2006) Homeostatic maintenance of ponderosa pine gas exchange in response to stand density changes. Ecol Appl 16:1164–1182.
McDowell N, Pockman WT, Allen CD et al. (2008) Mechanisms of plant survival and mortality during drought: why do some plants survive while others succumb to drought? New Phytol 178:719–739.
McDowell NG, Beerling DJ, Breshears DD, Fisher RA, Raffa KF, Stitt M (2011) The interdependence of mechanisms underlying climate-driven vegetation mortality. Trends Ecol Evol 26:523–532.
Meinzer FC, James SA, Goldstein G, Woodruff D (2003) Whole-tree water transport scales with sapwood capacitance in tropical forest canopy trees. Plant Cell Environ 26:1147–1155.
Nardini A, Battistuzzo M, Savi T (2013) Shoot desiccation and hydraulic failure in temperate woody angiosperms during an extreme summer drought. New Phytol 200:322–329.
Ogasa M, Miki NH, Murakami Y, Yoshikawa K (2013) Recovery performance in xylem hydraulic conductivity is correlated with cavitation resistance for temperate deciduous tree species. Tree Physiol 33: 335–344.
Palacio S, Maestro M, Montserrat–Martí G (2007) Seasonal dynamics of non–structural carbohydrates in two species of Mediterranean sub–shrubs with different leaf phenology. Environ Exp Bot 59:34–42.
Pantin F, Fanciullino AL, Massonnet C, Dauzat M, Simonneau T, Muller B (2013) Buffering growth variations against water deficits through timely carbon usage. Front Plant Sci 4:483.
Peguero-Pina JJ, Sancho-Knapik D, Martín P, Saz MA, Gea-Izquierdo G, Cañellas I, Gil-Pelegrín E (2015) Evidence of vulnerability segmentation in a deciduous Mediterranean oak (*Quercus subpyrenaica* E. H. del Villar). Trees 29:1917–1927.
Pellizzari E, Camarero JJ, Gazol A, Sangüesa-Barreda G, Carrer M (2016) Wood anatomy and carbon-isotope discrimination support long-term hydraulic deterioration as a major cause of drought-induced dieback. Glob Chang Biol 22:2125–2137.
Pflug EE, Siegwolf R, Buchmann N, Dobbertin M, Kuster TM, Günthardt-Goerg MS, Arend M (2015) Growth cessation uncouples isotopic signals in leaves and tree rings of drought-exposed oak trees. Tree Physiol 35:1095–1105.
Ponton S, Dupouey JL, Bréda N, Feuillat F, Bodénès C, Dreyer E (2001) Carbon isotope discrimination and wood anatomy variations in mixed stands of *Quercus robur* and *Quercus petraea*. Plant Cell Environ 24: 861–868.
Ragazzi A, Fedi ID, Mesturino L (1989) The oak decline: a new problem in Italy. Eur J For Path 19:105–110.
Ripullone F, Guerrieri MR, Saurer M, Siegwolf R, Jäggi M, Guarini R, Magnani F (2009) Testing a dual isotope model to track carbon and water gas exchanges in a Mediterranean forest. iForest 2: 59–66.
Roden JS, Farquhar GD (2012) A controlled test of the dual-isotope approach for the interpretation of stable carbon and oxygen isotope ratio variation in tree rings. Tree Physiol 32:490–503.
Roden JS, Siegwolf R (2012) Is the dual-isotope conceptual model fully operational? Tree Physiol 32:1179–1182.
Sala A, Piper FI, Hoch G (2010) Physiological mechanisms of drought-induced tree mortality are far from being resolved. New Phytol 186: 274–281.
Sala A, Woodruff DR, Meinzer FC (2012) Carbon dynamics in trees: feast or famine? Tree Physiol 32:764–775.
Salvatore M, Alessandro R, Irene D (2002) Current situation of oak decline in Italy and in other European countries. In Villemant C, Sousa E (eds) IOBC/WPRS Bulletin vol. 25. Working Group 'Integrated Protection in Oak Forests'. Lisbon, Portugal.
Sanders TGM, Pitman R, Broadmeadow MSJ (2014) Species-specific climate response of oaks (*Quercus* spp.) under identical environmental conditions. iForest 7:61–69.
Saurer M, Borella S, Leuenberger M (1997) $\delta^{18}O$ of tree rings of beech (*Fagus sylvatica*) as a record of $\delta^{18}O$ of the growing season precipitation. Tellus B 49:80–92.
Saurer M, Siegwolf R, Schweingruber F (2004) Carbon isotope discrimination indicates improving water-use efficiency of trees in northern Eurasia over the last 100 years. Glob Chang Biol 10:2109–2120.
Scheidegger Y, Saurer M, Bahn M, Siegwolf R (2000) Linking stable oxygen and carbon isotopes with stomatal conductance and photosynthetic capacity: a conceptual model. Oecologia 125:350–357.
Schneider CA, Rasband WS, Eliceiri KW (2012) NIH Image to ImageJ: 25 years of image analysis. Nat Methods 9:671–675.
Scholz A, Klepsch M, Karimi Z, Jansen S (2013) How to quantify conduits in wood? Frontiers Plant Sci 4:56.
Sevanto S, McDowell NG, Dickman LT, Pangle R, Pockman WT (2014) How do trees die? A test of the hydraulic failure and carbon starvation hypotheses. Plant Cell Environ 37:153–161.
Sperry JS, Nichols KL, Sullivan JEM, Eastlack SE (1994) Xylem embolism in ring-porous, diffuse-porous, and coniferous trees of Northern Utah and Interior Alaska. Ecology 75:1736–1752.
Stojanović D, Levanič T, Matović B, Bravo-Oviedo A (2015) Climate change impact on a mixed lowland oak stand in Serbia. Ann Silvicult Res 39:94–99.
Tessier L, Nola P, Serre-Bachet F (1994) Deciduous *Quercus* in the Mediterranean region—tree-ring/climate relationships. New Phytol 126:355–367.

Thomas FM, Hartmann G (1996) Soil and tree water relations in mature oak stands of northern Germany differing in the degree of decline. Ann Sci For 53:697–720.

Tognetti R, Longobucco A, Raschi A (1998) Vulnerability of xylem to embolism in relation to plant hydraulic resistance in *Quercus pubescens* and *Quercus ilex* co-occurring in a Mediterranean coppice in central Italy. New Phytol 139:437–447.

Tyree MT, Zimmermann MH (2002) Xylem structure and the ascent of sap. Springer, Berlin, Germany.

Vicente-Serrano SM, Beguería S, López-Moreno JI (2010) A multiscalar drought index sensitive to global warming: the Standardized Precipitation Evapotranspiration Index. J Clim 23: 1696–1718.

Villar-Salvador P, Castro-Díez P, Pérez-Rontomé C, Montserrat-Martí G (1997) Stem xylem features in three *Quercus* (Fagaceae) species along a climatic gradient in NE Spain. Trees 12:90–96.

Voltas J, Camarero JJ, Carulla D, Aguilera M, Oriz A, Ferrio JP (2013) A retrospective, dual-isotope approach reveals individual predispositions to winter-drought induced tree dieback in the southernmost distribution limit of Scots pine. Plant Cell Environ 36:1435–1448.

Williams AP, Allen CD, Macalady AK et al. (2013) Temperature as a potent driver of regional forest drought stress and tree mortality. Nat Clim Chang 3:292–297.

Wyckoff PH, Bowers R (2010) Response of the prairie–forest border to climate change: impacts of increasing drought may be mitigated by increasing CO_2. J Ecol 98:197–208.